Analytical Modeling of Location and Contention Randomness for Node-Assisted WiFi Backscatter Communication

Yulei Wang, Qinglin Zhao, *Senior Member, IEEE*, Shumin Yao, MengChu Zhou, *Fellow, IEEE*, Li Feng, and Peiyun Zhang, *Senior Member, IEEE*

***Abstract*— Node-assisted WiFi backscatter communication (NWB) is a promising technology that allows backscatter tags to communicate over long distances and achieve high throughput by using WiFi nodes as relays and enabling concurrent transmissions. However, NWB lacks an accurate theoretical model to evaluate and optimize its network performance, which is challenging to develop due to the location and contention randomness of both WiFi nodes and backscatter tags. Existing backscatter models that only account for one type of randomness are not suitable for NWB. To address this issue, we propose a novel stochastic geometry-based model that captures Location and Contention Randomness as well as the involved dependency and interference (named LoCoR). We use the Matérn hard-core point process and Matérn cluster process to model the repulsive and clustering attributes of the locations of WiFi nodes and backscatter tags, respectively. We also introduce a unified time unit to analyze the randomness and dependency of WiFi and backscatter contentions. Our model factors in various design parameters (e.g., the density and transmission power of tags) and can be used to evaluate their impacts on system throughput. We conduct extensive simulations to validate the accuracy of our model. With our accurate model, one can easily configure the optimal design parameters to maximize system throughput.**

***Index Terms*—WiFi backscatter communication, stochastic geometry, Matérn hard-core point process, Matérn cluster process, performance analysis**

I. INTRODUCTION

TO date, WiFi networks have been extensively deployed in indoor and outdoor environments, offering widespread connectivity and strongly supporting Internet-of-Things applications. WiFi backscatter communication [1], [2] exploits these ubiquitous WiFi signals as excitation signals to convey data and hence have broad application prospects in many fields [3], [4], [5]. Most existing studies of WiFi backscatter focus on one-hop communications between one WiFi device and backscatter tags (called tags for short) [1], [2], [6]. However, tags typically have very short transmission ranges (e.g., 1m to 54m [1], [7]) and low throughput, which greatly limits their practical deployments. Nevertheless, WiFi nodes (called nodes for short) possess much longer transmission ranges, which can be up to 1000m [8], [9], than backscatter tags. Recognizing this potential, Wang *et al.* [10] have recently proposed a node-assisted WiFi backscatter communication (NWB) scheme to extend tags' transmission range and improve the backscatter throughput.

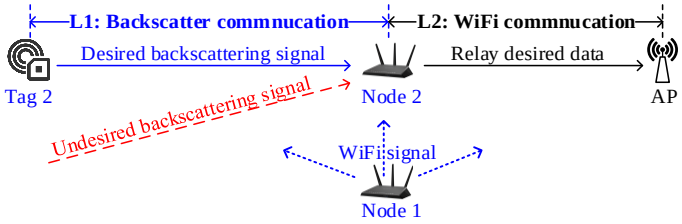

Fig. 1. An example of node-assisted WiFi backscatter.

A typical NWB network, as shown in Fig. 1, consists of one access point (AP), multiple randomly distributed WiFi nodes and many backscatter tags. In NWB, tags' data transmission passes through two-level communications: tag-to-node backscatter-level and node-to-AP WiFi-level communications. Consider the scenario that tag 2 intends to send its data to AP via its node (i.e., node 2). In backscatter communications, assume that node 1 is transmitting WiFi signals to AP. Regarding these WiFi signals as excitation signals, tag 2 first wins the channel and then transmits its data to node 2 by backscattering these excitation signals. In WiFi-level communications, node 2 also first wins the channel and then relays tag 2's data to AP, where node 2's transmissions, just like node 1's transmissions, can be regarded as excitation signals by other nodes' tags. Essentially, while one node is relaying its received tag data to a remote AP, the ongoing WiFi signal triggers multiple tags to transmit their data to their respective nodes concurrently. As a result, NWB can extend tags' transmission range and improve backscatter throughput.

Manuscript received August 4, 2023; revised January 17, 2024. This work is supported by the Science and Technology Development Fund, Macau SAR (0093/2022/A2, 0076/2022/A2, and 0008/2022/AGJ) and the National Key Research and Development Program of China (2023YFB2703800). (*Corresponding author: Q. Zhao.*)

Y. Wang, Q. Zhao and L. Feng are with the School of Computer Science and Engineering, Faculty of Innovation Engineering, Macau University of Science and Technology, Avenida Wei Long, Taipa, Macau, China (e-mail: wylpaper@126.com, qlzhao@must.edu.mo and lfeng@must.edu.mo).

S. Yao is with the School of Computer Science and Engineering, Macau University of Science and Technology, Avenida Wei Long, Taipa, Macau, China, and also with the Department of Broadband Communication, Peng Cheng Laboratory, Shenzhen 518066, China (e-mail: zhysm@outlook.com).

M.C. Zhou is with the Department of Electrical and Computer Engineering, New Jersey Institute of Technology, Newark, NJ 07102 USA (e-mail: zhou@njit.edu).

P. Zhang is with the Engineering Research Center of Digital Forensics of Ministry of Education, and the School of Computer Science, Nanjing University of Information Science & Technology, Nanjing 210044, China (email: zpy@nuist.edu.cn; 20211220029@nuist.edu.cn).

A. Motivation

NWB is a long-range and high-throughput technology. However, NWB lacks an accurate theoretical model that serves as a foundation for its performance evaluation and optimization. Nevertheless, developing such a model is by no means easy since it involves modeling the two types of random factors:

- Location randomness and dependency: In NWB, nodes are randomly deployed around AP and their deployment is of repulsive attributes, while tags are randomly deployed around nodes and their deployment is of clustering attributes.
- Contention randomness and dependency: In NWB, tags belong to different nodes and there are two-level contentions. In the WiFi level, nodes contend for transmitting their data to AP. In the backscatter level, tags depend on nodes' transmissions for their contentions and transmissions in their respective clusters. These concurrent transmissions cause interference while improving backscatter throughput.

Modeling NWB accurately needs to jointly consider the randomness and dependency of location and contention, as well as the interference due to concurrent transmissions. However, existing backscatter models, which consider either one type of randomness, or one type of dependency, or interference only, are not applicable for NWB. This motivates us to develop a comprehensive and accurate theoretical model to evaluate and optimize NWB network performance.

B. Our Contributions

This study proposes LoCoR as a novel stochastic geometry-based theoretical model for analyzing WiFi and backscatter throughputs of an NWB network. This study intends to make the following new contributions to advance the state of the art.

- It characterizes the location and contention randomness of WiFi nodes and backscatter tags in NWB, as well as the involved dependency and interference. For the location randomness, it employs Matérn hard-core point process and Matérn cluster process to capture the repulsive and clustering attributes of the locations of WiFi nodes and backscatter tags, respectively. For contention randomness, it introduces a unified unit time to clarify the dependency between WiFi and backscatter contentions.
- It expresses WiFi and backscatter throughputs analytically. The expressions factor in various design parameters, which are closely related to the randomness and dependency of WiFi nodes' and backscatter tags' locations and contentions, such as the density of nodes and tags, and transmission time of WiFi and backscatter data.
- It performs extensive simulations that verify the accuracy of our theoretical model and investigates the impacts of various design parameters on WiFi and backscatter throughputs.

LoCoR can help one select appropriate parameter settings to improve NWB throughput and optimize NWB performance.

The rest paper is organized as follows. Section II presents the related work. Section III outlines the network topology and Medium Access Control (MAC) layer protocol of an NWB network. Section IV specifies the system model. Sections V and VI give the theoretical analysis of WiFi and backscatter throughputs, respectively. Section 0 verifies the accuracy of our theoretical models via extensive simulations. Finally, Section VIII concludes the paper.

II. Related Work

Backscatter communication is a wireless communication technique that allows tags to communicate by exploiting their surrounding ambient signals to convey data without requiring any active radiofrequency (RF) components. WiFi backscatter communication is a type of backscatter network that utilizes existing WiFi infrastructures and ubiquitous WiFi signals to transmit data, making it ideal for use in Internet-of-Things (IoT).

The performance of backscatter communication is largely influenced by transmission interference, locations of tags, and adopted contention algorithms. Prior studies such as [11], [12] have well surveyed performance models of transmission interference. Here, we mainly outline the related ones from the perspective of location and contention randomness.

A. Modeling Location Randomness of Backscatter Networks

The models that study the location randomness of backscatter networks are largely developed based on stochastic geometry, which is about the study of random spatial patterns. Existing studies mainly investigate the performances of single-link or concurrent point-to-point backscatter transmissions. For instance, the model in [13] analyzes the overall backscatter energy and transmission outage probabilities in a single-link backscatter transmission from a tag to a reader on a laser-powered unmanned aerial vehicle. The location distributions of tags and laser-based charging stations are captured by homogeneous Poisson point and Poisson line Cox processes, respectively. In contrast, the model in [14] characterizes the location distributions of tags and analyzes their impacts on successful transmission probability of tags for concurrent point-to-point backscatter transmissions by using a homogeneous Poisson point process (HPPP). Additionally, the models in [15] and [16] utilize the Poisson cluster process to capture the location randomness of tags with spatial correlation for analyzing the impact of tags' location and concurrent transmissions on network performance. However, these models are proposed for analyzing scheduled point-to-point backscatter transmissions that do not occur in NWB with contention transmissions although they adopt spatial random processes to capture the location randomness of tags. Therefore, they are not applicable to NWB.

B. Modeling Contention Randomness of Backscatter Networks

Recent hardware advancements have enabled tags to adopt backoff-like contention algorithms for backscatter communication, which facilitate flexible and efficient transmissions in backscatter networks. Existing studies primarily investigate the randomness of pure or hybrid backscatter contention in backscatter communication. For example, Cao *et al.* [17] study an IoT network which allows multiple tags to connect with each other by relying on the ambient RF signal. They develop an enhanced 3-D Markov model to characterize the pure backscatter contention with dual-backoff mechanism, taking into account the tags' channel sensing errors. Additionally, some models have been proposed to capture the randomness of the hybrid backscatter contentions in backscatter networks. For example, the model in [18] considers an opportunistic backscatter

network where tags are allowed to perform binary exponential backoff (BEB) contention mechanism for conveying data to a reader, only when a hybrid AP is transmitting a wireless energy signal to the winner of IoT devices' contention. Furthermore, the models in [6] and [19] consider a type of WiFi backscatters that allow tags to perform contentions by using BEB algorithm in restricted periods won by a WiFi AP in its contention with other WiFi nodes. However, most of them focus on the cases where two types of contentions are governed by a dedicated device (i.e., AP), which is sharply different from NWB with two-level WiFi and backscatter contentions. Hence, they are not applicable to NWB.

C. Jointly Modeling Contention and Location Randomness of Backscatter Networks

To the best of our knowledge, the short version of this paper [20] is the only work that models both the contention and location randomness of WiFi backscatter networks. More specifically, it considers a WiFi backscatter network where tags contend by using a backoff algorithm for transmitting data to a WiFi node. For the location randomness, it adopts two independent HPPPs to describe the location distributions of WiFi nodes and backscatter tags, respectively. However, the two HPPPs fail to capture the repulsive and clustering characteristics of the locations of nodes and tags, respectively. For the contention randomness, [20] derives the contention successful probability for each tag. However, it does not account for the randomness of WiFi contention, and the dependency between backscatter and WiFi contentions. Therefore, this model is not applicable to NWB.

To summarize, existing backscatter-related models are not applicable to NWB because they do not thoroughly and jointly capture contention randomness, location randomness in backscatter networks, as well as the involved dependency. To address this issue, we propose a new analytical model called LoCoR.

III. Node-Assisted WiFi Backscatter Communication

This section describes the network topology of a node-assisted WiFi backscatter (NWB) network and outlines its MAC layer protocol [10].

A. Network Topology

A typical NWB network, as shown in Fig. 2, consists of one access point (AP), multiple randomly distributed WiFi nodes (called nodes for short) and many backscatter tags. The coverage of the AP is a circular *cell* and it serves all nodes in the cell. The coverage of a node is a circular *subcell* and it serves all tags in its subcell. For example, the AP serves nodes N1, N2, and N3, while N2 serves T3 and T4.

B. MAC Layer Protocol

In an NWB network, the AP, nodes, and tags are half-duplex (i.e., each device either transmits or receives at the same time). Its MAC layer protocol consists of WiFi and backscatter-level protocols. The latter is designed based on the former, since the backscatter tags exploit the node-to-AP WiFi signals as excitation signals to transmit tag-to-node data. With the help of Fig. 3, we explain the two protocols.

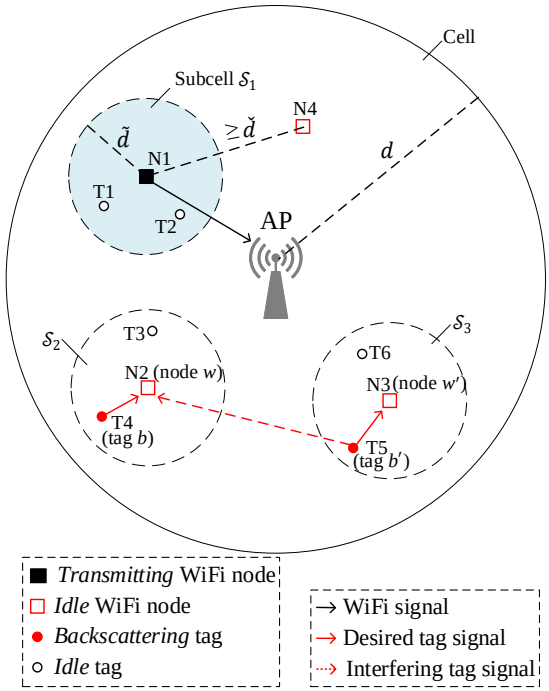

Fig. 2. A cell in an NWB network.

1) WiFi-level Protocol

In WiFi-level communications, nodes first contend for the channel and then the winner transmits its data. In contention, nodes adopt a carrier-sense multiple access with collision avoidance mechanism and a binary exponential backoff algorithm to alleviate the contention collision. At the beginning of contention, each node chooses a backoff count (BO) uniformly distributed in $[0, \check{C}-1]$, where $\check{C}$ is the minimum contention window size. After sensing the channel idle for a distributed interframe space (DIFS) time, it decreases its counter by one for each idle basic slot (i.e., a fixed minimum time unit) and suspends its counter for each busy basic slot. If its counter reaches zero, it transmits a packet to the AP and then waits for receiving an acknowledge (ACK) after a short interframe space (SIFS) time. If it cannot receive an ACK within a certain time (i.e., AckTimeout time), it infers that it experiences a collision. In case that a collision occurs, it doubles its contention window and enters a new backoff stage to retransmit the packet. When the backoff stage limit is reached, it either transmits the packet successfully or drops the packet. In the example, N1's and N2's BOs are 4 and 7, respectively and N1 wins the contention and then transmits since its BO is the minimum one.

To assist tag-to-node communications, the WiFi-level protocol makes some modifications on the structure of a conventional WiFi packet. As shown in Fig. 3, a WiFi packet comprises three parts:

- Header. This part comprises a PHY preamble, a PHY header and an MAC header. It is the same as a conventional WiFi packet header except adding some additional fields such as signature (i.e., a special sequence). Each node has a unique signature and will add it to the packet header when transmitting a packet to the AP.
- L identical busy tones. This is a newly added part. Each busy tone is a dedicated sequence. Upon detecting a busy tone, tags start contention. A busy tone duration denotes

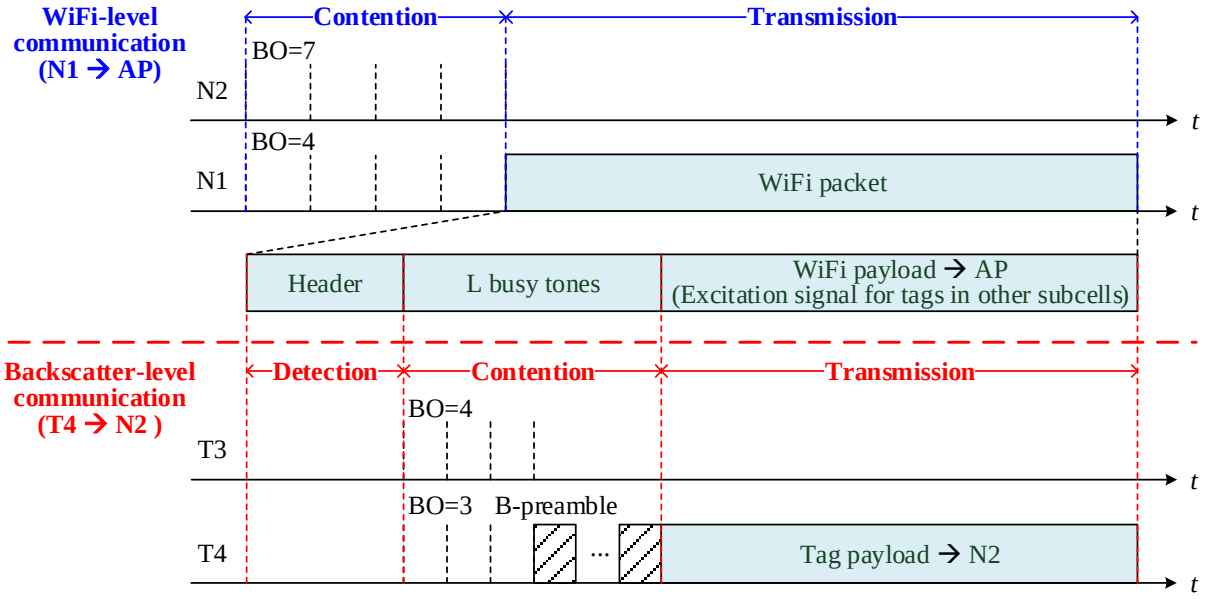

Fig. 3. An example of node-assisted tag transmissions in an NWB network.

the minimum time unit in the tag contention process. L denotes the contention window size of tags (i.e., the maximum number of time units in contention).

- WiFi payload. This part is the same as the conventional WiFi payload. The payload-transmission signal can be exploited as excitation signal of tags.

2) Backscatter-level Protocol

One backscatter communication process, as shown in Fig. 2 and Fig. 3, consists of three stages: detection, contention, and transmission. They correspond to the transmission stages of a WiFi packet's three parts: header, L identical busy tones, and WiFi payload, respectively.

In detection, each tag correlates its buffered node signatures with the received signal to detect if its node or other nodes are transmitting a WiFi packet. If the transmitting node is its node, it first calculates the transmission duration of the whole WiFi packet according to the duration field of the packet, and then remains idle until the next packet transmission. Otherwise, it harvests sufficient energy in the detection stage and then enters the contention and transmission stages. For example, in Fig. 2, T1 and T2 find that their node N1 is transmitting and hence keep idle in N1's transmission process. In contrast, T3 and T4 find that their node N2 does not transmit and hence harvest energy only in the detection stage.

In contention, each tag exploits the busy tones to perform contention and the winner transmits a predefined backscatter preamble (called B-preamble for short), which is unique for each subcell. At the beginning of contention, each tag chooses a BO uniformly distributed in $[0, L-1]$ and then starts counting down. For each time unit in contention, each tag performs two types of correlations: busy-tone and B-preamble correlations. If it detects a busy tone only, it decreases its counter by one. In contrast, whenever it detects a B-preamble, it stops contention and remains idle until the end of the backscatter communication. When its counter reaches zero, it keeps broadcasting B-preamble until the end of the contention stage. For example, T3's and T4's initial BOs are 4 and 3, respectively. Hence T4 will win the contention and broadcast the B-preamble.

In transmission, the winning tag transmits its data to its node. For example, T4 transmits its data to N2. A node may receive three types of signals as shown in Fig. 1: (i) the WiFi signal, (ii) the desired tag signal, and (iii) the interfering tag signals. By exploiting the successive interference cancellation technology [21], [22], the node can first recognize and remove the WiFi signal, and then decode the desired signal from the remaining superposed signals [10].

IV. LoCoR Model

In this section, we specify LoCoR in terms of the spatial distributions of nodes and tags, the energy harvesting of tags, the interference and channel model, traffic model, and system throughput. All the used notations are summarized in TABLE I in Appendix A of Supplementary File [23].

A. Spatial Distribution

As shown in Fig. 2, we focus on a single-cell NWB network, where all nodes can hear each other. We use $A \subset \mathbb{R}^2$ with radius d to denote a circular *cell*. The cell consists of one AP, multiple nodes and numerous tags.

1) Matérn Hard-Core Point Process of Nodes

We employ Matérn hard-core point process of type II (called MHCPP for short) $\Phi_w \subset \mathbb{R}^2$ to model the spatial location distribution of nodes, which effectively captures the repulsive characteristics among nodes in a practical network. Specifically, an MHCPP Φ_w of nodes [24] is generated from a dependent thinning of homogeneous Poisson point process (HPPP) $\Phi_w^0 = \{\mathbf{x_i}, i \in \mathbb{N}^+\} \subset \mathbb{R}^2$ of nodes with density λ_w^0, i.e., λ_w^0 nodes in a unit area. First, each node $\mathbf{x_i} \in \Phi_w^0$ is marked independently with a random label M_i where M_i is uniformly distributed in the interval $[0, 1]$. Then, $\mathbf{x_i} \in \Phi_w^0$ is retained in Φ_w if $\mathcal{D}(\mathbf{x_i}, \check{d})$ does not contain any point of Φ_w^0 with label smaller than M_i. The retained nodes form an MHCPP Φ_w, i.e.,

$$\Phi_w \triangleq \{\mathbf{x_i} \in \Phi_w^0 : M_i < M_j, \forall\, \mathbf{x_j} \in \Phi_w^0 \cap \mathcal{D}(\mathbf{x_i}, \check{d}) \backslash \mathbf{x_i}\}$$

where $\mathcal{D}(\mathbf{x_i}, \check{d})$ represents a disk centered at node $\mathbf{x_i} \in \Phi_w^0$ with radius $\check{d}$, and $\check{d}$ represents the minimum distance between any two nodes. Let p_w denote the probability that a random node $\mathbf{x_i} \in \Phi_w^0$ can be retained in Φ_w. According to [25], p_w is expressed as

$$p_w = \begin{cases} \dfrac{1-\exp\left(-\lambda_w^0 \pi \check{d}^2\right)}{\lambda_w^0 \pi \check{d}^2} & \check{d} > 0 \\ 1 & \check{d} = 0 \end{cases}, \tag{1}$$

and the corresponding density λ_w of Φ_w can be obtained by weighting λ_w^0 with p_w, i.e.,

$$\lambda_w = p_w \lambda_w^0 \tag{2}$$

As studied in [24], [26], [27], [28], MHCPP Φ_w can be further approximated as HPPP Φ_w^a with same density λ_w, i.e.,

$$\Phi_w^a \approx \Phi_w \tag{3}$$

and the accuracy of such approximation is validated in [29]. Hence, the nodes within cell A are assumed to approximately follow uniform distribution in location and Poisson distribution with mean $\lambda_w|A|$, where $|A| = \pi d^2$ denotes the area of one cell. We use $\tilde{A} \subset \mathbb{R}^2$ with radius $\tilde{d}$ to denote a circular *subcell*, which is formed by one node.

2) Matérn Cluster Process of Tags

We employ the Matérn cluster process (MCP) $\Phi_b \subset \mathbb{R}^2$ to model the spatial location distribution of tags, which effectively captures the clustering characteristics of tags in a practical network [15]. According to [30], we can generate:

$$\Phi_b \triangleq \bigcup_{\mathbf{x_i} \in \Phi_w^a} \Phi_i + \mathbf{x_i} \tag{4}$$

where Φ_w^a is an HPPP defined in (3), and the offspring tags $\mathbf{y_i} \in \Phi_i$ are uniformly scattered in the subcell $\mathcal{D}(\mathbf{x_i}, \tilde{d})$ centered at a parent node $\mathbf{x_i} \in \Phi_w^a$ with radius $\tilde{d}$, and follow Poisson distribution with mean Λ_b [31]. Let $\mathbf{x}$ and $\mathbf{y}$ respectively denote the Cartesian coordinates of a parent node and its one offspring tag, where the distribution of offspring tags around the parent node in each subcell are independent and identically distributed (i.i.d.) with the same spatial probability density function (PDF). Given an $\mathbf{x}$, the conditional PDF of $\mathbf{y}$, $f(\mathbf{y}|\mathbf{x})$, is expressed as

$$f(\mathbf{y}|\mathbf{x}) = \begin{cases} \dfrac{1}{\pi \tilde{d}^2}, \|\mathbf{y}-\mathbf{x}\| \le \tilde{d} \\ 0, \quad otherwise. \end{cases} \tag{5}$$

Let R_y represent the Euclidean distance between an offspring tag $\mathbf{y}$ and its parent node $\mathbf{x}$, i.e., $R_y = \|\mathbf{y}-\mathbf{x}\|$. Since offspring tags are uniformly scattered in the subcell $\mathcal{D}(\mathbf{x}, \tilde{d})$ centered at $\mathbf{x}$, the cumulative distribution function (CDF) of R_y is given as:

$$\tilde{F}_{R_y}(r_y) = \mathbb{P}(R_y \le r_y) = \frac{\pi r_y^2}{\pi \tilde{d}^2} = \frac{r_y^2}{\tilde{d}^2}, 0 \le r_y \le \tilde{d}. \tag{6}$$

Hence, we can express the PDF of R_y as:

$$\tilde{f}_{R_y}(r_y) = \frac{d\tilde{F}_{R_y}(r_y)}{dr_y} = \frac{2r_y}{\tilde{d}^2}, 0 \le r_y \le \tilde{d}. \tag{7}$$

To facilitate the analysis, we give the probability generating functional (PGFL) of an MCP Φ_b in advance. For any function $v(\mathbf{y}): \mathbb{R}^2 \to [0,1]$ and $\int_{\mathbb{R}^2}(1-v(\mathbf{y}))\,d\mathbf{y} < \infty$, the PGFL of an MCP Φ_b is given as [30], [32], [33], [34]:

$$G(v) = \mathbb{E}\left[\prod_{\mathbf{y} \in \Phi_b} v(\mathbf{y})\right]$$
$$= \exp\left(-\lambda_w \int_{\mathbb{R}^2}\left[1-\exp\left(-\Lambda_b \int_{\mathbb{R}^2}(1-v(\mathbf{y}'+\mathbf{x}))f(\mathbf{y}'|\mathbf{x})d\mathbf{y}\right)\right]d\mathbf{x}\right) \tag{8}$$

where $\mathbf{x}, \mathbf{y} \in \Phi_b$ are coordinates with respect to the origin $\boldsymbol{o}(0,0)$, $\mathbf{y}'$ is the coordinate with respect to $\mathbf{x}$ where $\mathbf{y}'$ and $\mathbf{y}$ are different representations of the same point under different reference points, and $f(\mathbf{y}'|\mathbf{x})$ is given as that in (5).

B. Energy Harvesting of Tags

As shown in Fig. 3, a whole transmission process of a tag consists of three stages: detection, contention, and transmission. In this paper, to concentrate on our main contributions, we assume that each tag can harvest sufficient energy in the detection stage for contention and data transmission. On one hand, this assumption is feasible. For example, as shown in Fig. 3, we may add a special field (e.g., energy tones) after the WiFi header, so as to increase the detection time which spans the transmission time of the WiFi header and the special field. As long as the detection time is sufficiently long, tags can harvest sufficient energy in the detection stage. On the other hand, like [15], [16], we may extend our framework to model the number of tags that can harvest sufficient energy. For example, let Λ_b' denote the mean number of tags in each subcell which can harvest sufficient energy in the detection stage. Let p_b be the probability that one tag can harvest sufficient energy, which is related to the distance between energy emitters and the tag as well as the energy harvesting efficiency of the tag. Since Λ_b is the total mean number of tags in each subcell, we have $\Lambda_b' = p_b \Lambda_b$.

C. Interference and Channel Model

In an NWB network as shown in Fig. 2, when a node N1 in subcell $\mathcal{S}_1$ is transmitting a packet to the AP, tag b in subcell $\mathcal{S}_2$ may transmit its data to its node w by backscattering this N1-to-AP signal. In general, when one node in $\mathcal{S}_1$ transmits a WiFi signal to the AP, tags in all subcells except $\mathcal{S}_1$ may transmit their data to their respective nodes by backscattering this WiFi signal. Before proceeding with the interference model, we make two assumptions:

1. Tag transmissions will not interfere with the node-to-AP transmission. The reason is as follows. The received tag signal power at the AP is far less than the received node power [17], [35], and hence the AP may adopt successive interference cancellation [21], [22] to extract WiFi signals successfully. Because of Assumption 1, in this paper, we do not analyze the impact of tags' transmissions on WiFi throughput.

2. The node-to-AP WiFi transmission will not interfere with tag-to-node transmissions (say, the N1-to-AP transmission will not interfere with the b-to-w transmission), since node w may exploit successive interference cancellation to remove WiFi signal and further decode the desired b-to-w signal [10], [21], [22], as explained in the last paragraph of Section III.B.2).

In general, these WiFi and tag signals do not mutually interfere with each other.

However, when tag b in $\mathcal{S}_2$ transmits its data to its node w, other tag transmissions in other subcells such as $\mathcal{S}_3$ may interfere with this b-to-w transmission. Let $\Phi_b' \subset \Phi_b$ be a set of interfering tags that interfere with a desired tag transmission (e.g.,

the b-to-w tag transmission). Φ_b' does not contain the tags in the subcell where the node is transmitting a WiFi signal to the AP; for example, Φ_b' excludes the tags in $\mathcal{S}_1$. The interference level from Φ_b' depends on the location and number of nodes and tags is modeled in Section VI. To capture this impact of these interferences on the tag transmissions, we consider that each tag signal undergoes both large and small-scale channel fading [36]. We assume that the former follows a path loss model $r^{-\alpha}$, where r is the Euclidean distance between a tag and its node, and $\alpha, 2 < \alpha < 6$, is the path-loss exponent [15], [37]. We assume that each channel power gain H in the latter is independent and identically distributed with an exponential distribution with mean $1/\mu$, i.e., $H \sim \text{Exp}(\mu)$ [38], [39]. For example, consider the b-to-w transmission. Let P_0 denote the reflection power of each tag. Let $P_{b,w}$ denote the received signal power from tag b at the node w. Let $H_{b,w}$ and $R_{b,w}$ be the channel power gain and the distance between tag b and node w, respectively. According to the above channel model, we have:

$$P_{b,w} = P_0 H_{b,w} R_{b,w}^{-\alpha} \tag{9}$$

Further, let I denote the interference power that node w suffers, which is mainly from the interference of tags in Φ_b' due to Assumption 2. I can be expressed as

$$I = \sum_{b' \in \Phi_b'} P_0 H_{b',w} R_{b',w}^{-\alpha} \tag{10}$$

where $H_{b',w}$ and $R_{b',w}$ are the channel power gain and the distance between tag b' and node w, respectively.

In addition, we assume an additive white Gaussian noise channel with zero mean and variance σ^2.

D. Traffic Model

Like [40], [41], to investigate the system capacity, we assume saturated traffic, namely, each WiFi node and each tag always have data to transmit.

E. System Throughput

For an NWB network, under the above assumptions, we adopt a stochastic geometry approach to investigate its system throughput. We define the average system throughput Γ_s as the sum of the average WiFi throughput Γ_w and the average backscatter throughput Γ_b. That is,

$$\Gamma_s = \Gamma_w + \Gamma_b \tag{11}$$

In the following two sections, we calculate Γ_w and Γ_b sequentially. Particularly, our theoretical model captures the impact of the contention, location, and number of WiFi nodes on the backscatter throughput.

V. WiFi Throughput

This section analyzes the average WiFi throughput Γ_w.

Let ξ be the WiFi throughput representing the number of successfully transmitted bits by WiFi nodes in one cell, during a unit time. Let $\mathbb{E}[\xi]$ be the mean of ξ. Then we have

$$\Gamma_w \triangleq \mathbb{E}[\xi] \tag{12}$$

According to the WiFi-level protocol, nodes first contend for the channel successfully and then transmit packets. The number of nodes affects the probability of winning the contention and hence the WiFi throughput ξ. Let M denote the number of nodes in one cell. Let $\mathbb{P}(m) \triangleq \Pr(M = m)$ be the probability mass function of M. Recall that the nodes follow HPPP Φ_w^a with density λ_w defined in (3) and the number of nodes in one cell follows a Poisson distribution with mean $\lambda_w|A|$. Hence, $\mathbb{P}(m)$ is given as:

$$\mathbb{P}(m) = \exp(-\lambda_w|A|)\frac{(\lambda_w|A|)^m}{m!} \tag{13}$$

Then, according to the law of total expectation, we have:

$$\mathbb{E}[\xi] = \sum_{m=1}^{\hat{m}} \mathbb{P}(m)\,\mathbb{E}[\xi|m] \tag{14}$$

where m takes a value from 1 to a maximum value $\hat{m}$.

Next, we calculate $\mathbb{E}[\xi|m]$ by following the method in [40], [42], [43]. Let Ω denote a generic slot duration representing the elapsed time of one backoff decrement in WiFi contention. Let $\mathbb{E}[\Omega|m]$ denote the mean of Ω when m nodes contend for the channel and regard $\mathbb{E}[\Omega|m]$ as the unit time for calculating the average throughput $\mathbb{E}[\xi|m]$. Let $\mathbb{P}_w(Succ|m)$ denote the probability of a successful node-to-AP transmission when m nodes contend for the channel. Then, $\mathbb{E}[\xi|m]$ can be expressed as

$$\mathbb{E}[\xi|m] = \frac{\mathbb{P}_w(Succ|m) \cdot L_w}{\mathbb{E}[\Omega|m]} \tag{15}$$

where L_w is the average WiFi packet size (measured in bits). The calculation details of $\mathbb{P}_w(Succ|m)$ and $\mathbb{E}[\Omega|m]$ can be found in Appendix C of Supplementary File [23].

VI. Backscatter Throughput

This section analyzes the average backscatter throughput Γ_b.

Let η be the backscatter throughput representing the number of successfully transmitted bits by tags within all subcells, during a unit time. Let $\mathbb{E}[\eta]$ be the mean of η. Then we have

$$\Gamma_b \triangleq \mathbb{E}[\eta] \tag{16}$$

According to this definition, the average backscatter throughput is related to the number of all subcells. Since one node forms one subcell, the number of all nodes in a cell, m, is the number of all subcells. According to the law of total expectation, we have:

$$\mathbb{E}[\eta] = \sum_{m=1}^{\hat{m}} \mathbb{P}(m)\,\mathbb{E}[\eta|m] \tag{17}$$

where $\mathbb{P}(m)$ is the probability that there are m nodes in one cell and is given in (13), and m takes a value from 1 to a maximum value $\hat{m}$. Below, we give the expression of $\mathbb{E}[\eta|m]$.

We first model the unit time in the definition of the backscatter throughput. Recall that tags' transmissions depend on one node-to-AP transmission. For example, as shown in Fig. 2, when node N1 wins the WiFi-level contention and starts transmitting its packet to the AP, upon sensing this N1-to-AP signal, tags in each subcells except $\mathcal{S}_1$ first contend for the channel and then the winning tag transmits its data to its node, e.g., tag b in $\mathcal{S}_2$ transmits one data to node w. When analyzing the WiFi throughput in Section V, we use $\mathbb{E}[\Omega|m]$, which is given in (8) in Appendix C of Supplementary File [23], to denote the unit time. During the duration $\mathbb{E}[\Omega|m]$, if there is a node transmitting its packet to the AP, the winning tags can transmit their data to their respective nodes. Hence, we also use $\mathbb{E}[\Omega|m]$ to denote the unit time to calculate $\mathbb{E}[\eta|m]$.

Then, we express $\mathbb{E}[\eta|m]$. Let us focus on subcell $\mathcal{S}_2$ in Fig. 2 to first analyze the backscatter throughput in one subcell. Let $\mathbb{P}_b^s$ be the successful probability that a tag in one cell transmits one

data to its node (e.g., tag b in $\mathcal{S}_2$ transmits one data to node w). Then, the backscatter throughput in $\mathcal{S}_2$ can be expressed as $\frac{\mathbb{P}_b^S \cdot L_b}{\mathbb{E}[\Omega|m]}$, where L_b is the average backscatter data size (measured in bits). Now, we express the backscatter throughput of all subcells. Given m nodes in one cell, when one node in one cell transmits its packet to the AP, tags in $m-1$ subcells (except the subcell formed by the transmitting node) may transmit their data to their respective nodes in parallel. Hence, we have:

$$\mathbb{E}[\eta|m] = (m-1) \cdot \mathbb{P}_w(Succ|m) \cdot \frac{\mathbb{P}_b^S \cdot L_b}{\mathbb{E}[\Omega|m]} \tag{18}$$

where $\mathbb{P}_w(Succ|m)$ and $\mathbb{E}[\Omega|m]$ are given in (2) and (8) in Appendix C of Supplementary File [23]. Below, we calculate $\mathbb{P}_b^S$, which is related to both two types of randomness: (i) the contention randomness of tags in one subcell, and (ii) the location randomness of tags and nodes. Let us focus on $\mathcal{S}_2$ in Fig. 2 again. Let N denote the number of tags in $\mathcal{S}_2$. Let Ψ denote the number of tags that win and transmit in $\mathcal{S}_2$ simultaneously. Let $\mathbb{P}(\Psi=1, N=n)$ denote the probability that n tags are in $\mathcal{S}_2$ but only one tag wins the channel. Let $\mathbb{P}(RX\_succ|\Psi=1)$ denote the probability that the transmission of the winning tag is successfully received by its node, on condition that only one tag wins the channel and transmits in $\mathcal{S}_2$. Consider that tag b in $\mathcal{S}_2$ transmits one data to node w. According to the backscatter-level protocol, one successful b-to-w transmission should satisfy two conditions: (C1) only tag b wins the contention and transmits and (C2) tag b's transmission is successfully received by node w. Therefore, given $N=n$ tags in $\mathcal{S}_2$, one successful b-to-w transmission probability is $\mathbb{P}(\Psi=1, N=n) \cdot \mathbb{P}(RX\_succ|\Psi=1)$. Since N may take a value from 1 to the maximum value $\hat{n}$, we express $\mathbb{P}_b^S$ as:

$$\mathbb{P}_b^S = \sum_{n=1}^{\hat{n}} \mathbb{P}(\Psi=1, N=n) \cdot \mathbb{P}(RX\_succ|\Psi=1) \tag{19}$$

In (19), $\mathbb{P}(\Psi=1, N=n)$ is related to the contention randomness of tags in one subcell, while $\mathbb{P}(RX\_succ|\Psi=1)$ is related to the location randomness of tags and nodes. In the next two subsections, we calculate the two probabilities sequentially.

A. Probability That a Tag Wins & Transmits $\mathbb{P}(\Psi=1, N=n)$

For $1 \le \psi \le n$, we give a general expression of $\mathbb{P}(\Psi=\psi, N=n)$, from which we may calculate $\mathbb{P}(\Psi=1, N=n)$. Let $\mathbb{P}(n) \triangleq \Pr(N=n)$ be the probability mass function of N. Let $\mathbb{P}(\Psi=\psi|n)$ be the probability that ψ tags win the contention and transmit when n tags contend for the channel in one subcell. The joint probability of Ψ and N is given as:

$$\mathbb{P}(\Psi=\psi, N=n) = \mathbb{P}(n)\mathbb{P}(\Psi=\psi|n) \tag{20}$$

1) Calculation of $\mathbb{P}(n)$

Recall that the tags follow MCP Φ_b and the number of tags in each subcell follows a Poisson distribution with mean Λ_b. Hence, $\mathbb{P}(n)$ is given as:

$$\mathbb{P}(n) = \exp(-\Lambda_b)\frac{(\Lambda_b)^n}{n!} \tag{21}$$

2) Calculation of $\mathbb{P}(\Psi=\psi|n)$

According to the backscatter-level protocol, during the contention, each tag in a subcell uniformly chooses one backoff counter from 0,1, …, $L-1$ for countdown, where L is the number of busy tones. The tag that chooses the minimum backoff counter is the winner. Let l, $l=0,1,\dots,L-1$, denote the minimum backoff counter in one contention process. Depending on whether ψ is equal to n, we have

$$\mathbb{P}(\Psi=\psi|n) = \begin{cases} L\left(\frac{1}{L}\right)^{\psi} & \psi = n \\ \sum_{l=0}^{L-2} \binom{n}{\psi}\left(\frac{1}{L}\right)^{\psi}\left(\frac{L-1-l}{L}\right)^{n-\psi} & \psi < n \end{cases} \tag{22}$$

A detailed explanation of (22) is as follows. When $\psi = n$, each tag chooses the same l with probability $1/L$ and hence all tags are all winners with probability $(1/L)^{\psi}$. Since l may take L values from 0 to $L-1$, we obtain the top expression in (22).

When $\psi < n$, ψ tags are winners and at least one tag is the loser. Each of ψ tags chooses the same l with probability $1/L$, while each of the remaining $n-\psi$ tags chooses one backoff count from $l+1$ to $L-1$ with probability $(L-1-l)/L$. Taking into account all possible values that l may take and the combination number of tags being winners $\binom{n}{\psi}$, we obtain the bottom expression in (22). For an intuitive illustration of the calculation of (22), please refer to Appendix D of Supplementary File [23].

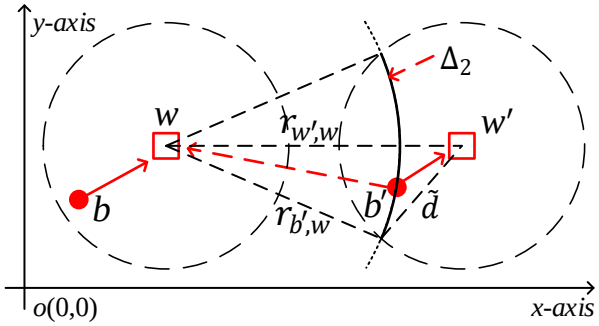

Fig. 4. Node w's received desired signal from tag b and interfering signal from tag b'.

B. Probability That a Tag-to-node Transmission is Successfully Received $\mathbb{P}(RX\_succ|\Psi=1)$

In a tag-to-node transmission, as shown in Fig. 4, a node $w \in \Phi_w$ receives a desired signal from a tag $b \in \Phi_b$ in $\mathcal{S}_2$ and interfering signals from interfering tags $b' \in \Phi_b' \subset \Phi_b$ when b' is transmitting to its node $w' \in \Phi_{w'} \subset \Phi_w$, where $\Phi_{w'}$ represents the set of non-transmitting nodes except node w. In a point process, with probability one, no two or more points coincide in the same location (or coordinate) [44]. In this paper, when mentioning a node w, we mean that the node is located in the coordinate w that is also used to denote the node itself. In Fig. 4, the coordinates, w, w', b and b' are under the same reference point $o(0,0)$ in a two-dimensional plane.

Let $R_{b,w}$ denote the distance between tag b and node w. Let I denote the power of the interference that node w suffers, where I is given in (10). Let $SINR(R_{b,w}, I)$ denote the signal-to-interference-plus-noise ratio (SINR) between node w's received power of the desired signal from tag b, $P_{b,w}$, and its suffered interference power I plus noise power σ^2. We may express $SINR(R_{b,w}, I)$ as:

$$SINR(R_{b,w}, I) = \frac{P_{b,w}}{I+\sigma^2} = \frac{P_0 H_{b,w} R_{b,w}^{-\alpha}}{I+\sigma^2} \quad (23)$$

where $P_{b,w}$ is given in (9) and is a function of tag b's reflection power P_0, the channel power gain $H_{b,w}$, and the distance $R_{b,w}$.

In our model, node w successfully receives a signal from tag b if its measured SINR exceeds a predefined threshold θ (i.e., $SINR(R_{b,w}, I) > \theta$). Thus, we have:

$$\mathbb{P}(RX\_succ|\Psi = 1) = \mathbb{E}_{I,R_{b,w}}\left[\mathbb{P}\left(SINR(R_{b,w}, I) > \theta\right)\right]$$
$$= \int_0^{\tilde{d}} \mathbb{E}_I\left[\mathbb{P}\left(SINR(r_{b,w}, I) > \theta\right)\right] \cdot \tilde{f}_{R_{b,w}}(r_{b,w}) dr_{b,w} \quad (24)$$

where $\tilde{d}$ is the radius of a subcell, $\tilde{f}_{R_{b,w}}(r_{b,w})$ is the PDF of $R_{b,w}$. According to the definition of MCP, $\tilde{f}_{R_{b,w}}(r_{b,w})$ is expressed as that in (7).

We then express $\mathbb{E}_I\left[\mathbb{P}\left(SINR(r_{b,w}, I) > \theta\right)\right]$ in (24) as

$$\mathbb{E}_I\left[\mathbb{P}\left(SINR(r_{b,w}, I) > \theta\right)\right] = \mathbb{E}_I\left[\mathbb{P}\left(\frac{P_0 H_{b,w} r_{b,w}^{-\alpha}}{I+\sigma^2} > \theta\right)\right]$$
$$= \exp(-s\sigma^2) \cdot \mathcal{L}_I(s) \quad (25)$$

where $s = \frac{\mu\theta r_{b,w}^{\alpha}}{P_0}$. Note that I is the interference that node w suffers depends on the set of interfering tags Φ_b'. $\mathcal{L}_I(s)$ is the Laplace transform of interference I. It has an asymptotic lower bound, $\mathcal{L}_I'(s)$, when $\check{d} \to 0$, $d \to \infty$:

$$\mathcal{L}_I'(s) = \exp\left(-\pi\lambda_w'\bar{\Psi} r_{b,w}^2 \theta^{\frac{2}{\alpha}} \frac{1}{\mathrm{sinc}(2/\alpha)}\right), \quad (26)$$

where λ_w' is the density of nodes w' forming the subcells that contain interfering tags of Φ_b', $\bar{\Psi}$ is the mean of Ψ.

The details of $\mathcal{L}_I(s)$ and $\mathcal{L}_I'(s)$ can be found in Appendix E of Supplementary File [23].

VII. Model Verification

We conduct extensive simulations to verify the accuracy of our theoretical model and compare our model with that in [10], which assumes ideal channel conditions and does not consider the location distribution characteristics of nodes and tags, and ignores the interferences.

Our simulator is developed based on MATLAB 2018a. This simulator integrates the MAC module of NWB from [10], the white Gaussian noise generator module, the spatial distribution module in Section III.A and the channel module in Section III.C. We set WiFi parameters according to [8] and NWB parameters according to [10]. Each simulation value is obtained from a simulation run of 400 seconds; a longer simulation time just yields negligible fluctuations. In all figures, the labels 'ana' and 'sim' denote the theoretical and simulation results, respectively. The default parameter settings of simulation can be found in Table II in Appendix F of the Supplementary File [23].

A. System Throughput

We now verify the accuracy of the system throughput Γ_s, WiFi throughput Γ_w, and backscatter throughput Γ_b when λ_w and Λ_b varies, under $\alpha = 3$, $L = 8$, $\tilde{d} = 7$ m, $\check{d} = 10$ m, $\theta = 10$ dB, $P_0 = 1$ dBm and $\sigma^2 = -100$ dBm, and compare them with those in [10] and [20]. For all figures in this subsection, labels 'Sys.', 'WiFi', 'BScatt.', '[10]', '[20]' and 'ours' denote the system throughput, WiFi throughput, backscatter throughput, results in [10], [20] and results in our work, respectively.

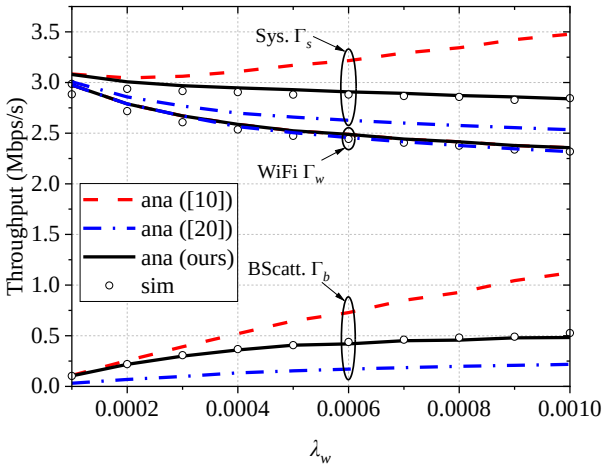

Fig. 5. Γ_s, Γ_w, and Γ_b versus λ_w under $\Lambda_b = 3$.

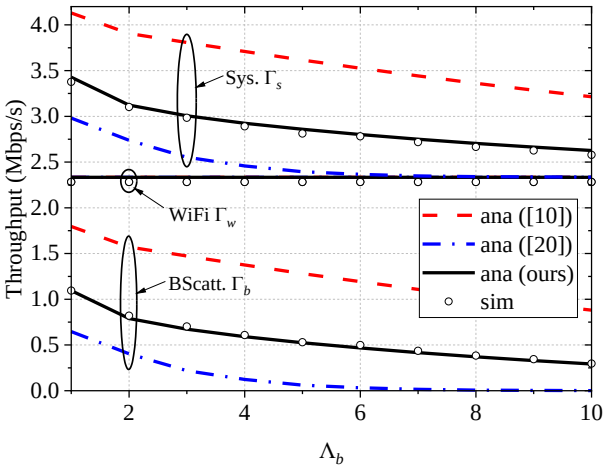

Fig. 6. Γ_s, Γ_w, and Γ_b versus Λ_b under $\lambda_w = 0.001$ nodes/m^2.

Fig. 5 shows the impacts of different λ_w on Γ_s, Γ_w, and Γ_b, when $\Lambda_b = 3$. From this figure, we can conclude:

1) Given Λ_b, Γ_b increases as λ_w increases. The reason is that as λ_w increases, the number of nodes serving tags increases, thereby contributing to more concurrent tag-to-node transmissions and increasing Γ_b.
2) Given Λ_b, Γ_w decreases as λ_w increases. The reason is that as λ_w increases, the number of nodes increases, which leads to more contention collisions, hence Γ_w decreases.
3) Given Λ_b, Γ_s first decreases from 0.0001 to 0.0002 nodes/m^2 and then increases as λ_w increases from 0.0002 to 0.001 nodes/m^2 in [10]. The reason is as follows. Recall that $\Gamma_s = \Gamma_w + \Gamma_b$. As λ_w increases from 0.0001 to 0.0002 nodes/m^2, the decrease amount of Γ_w is slightly larger than the increase amount of Γ_b. However, as λ_w increases from 0.0002 to 0.001 nodes/m^2, the decrease amount of Γ_w is smaller than the increase amount of Γ_b. In contrast, Γ_s always decreases as λ_w increases in our work and [20], because the decrease amount of Γ_w is larger than the increase amount of Γ_b.

Fig. 6 plots the impacts of different Λ_b on Γ_s, Γ_w, and Γ_b as Λ_b varies, when $\lambda_w = 0.001$ nodes/m^2. From this figure, we can conclude:

1) Given λ_w, Γ_w remains unchanged as Λ_b increases, indicating Λ_b does not impact WiFi-level communication.

2) Given λ_w, Γ_b decreases as Λ_b increases. The reason is that as Λ_b increases, the number of interfering links increases, which decreases the successful transmission probability of tags.
3) Given λ_w, Γ_s decreases as Λ_b increases, because Γ_s is the sum of unchanged Γ_w and decreased Γ_b.

In addition, from both Figs. 5-6, we further conclude that:

4) Our theoretical results closely match the corresponding simulation ones, which verifies the accuracy of our model; while the theoretical results of [10] and [20] do not.
5) For system and backscatter throughputs, the results in [10] and [20] are significantly different from our results. The reasons are as follows: 1) the model in [10] assumes ideal channel conditions and considers neither the spatial distributions of nodes and tags nor the impact of the interferences on the system throughput, and 2) the model in [20] assumes that the location distributions of nodes and tags follow two independent HPPPs, thereby ignoring the repulsive attributes of WiFi nodes and the clustering attributes of backscatter tags.
6) For WiFi throughput, our results are the same as those in [10] and [20], because we mainly investigate the impact of WiFi contention on backscatter transmissions and hence adopt the same settings (including ideal channel conditions) as those in [10] and [20] to reduce the analysis complexity.

B. Successful Transmission Probability

We verify the accuracy of successful transmission probability $\mathbb{P}_b^s$ in (*19*). Fig. 7 shows the impacts of different λ_w^0 (i.e., λ_w^0 = 0.0005, 0.001, 0.002 nodes/m^2) on $\mathbb{P}_b^s$ as $\check{d}$ varies from 0 to 20 m. Besides, $\alpha = 3$, $L = 8$, $\Lambda_b = 5$, $\theta = 10$ dB, $P_0 = 1$ dBm, and $\sigma^2 = -100$ dBm. From this figure, we can conclude:

1) Given λ_w^0, $\mathbb{P}_b^s$ increases as $\check{d}$ does. It is because that the larger $\check{d}$, the smaller density λ_w of retained nodes, and the smaller the number of retained nodes in the cell, the fewer the total number of transmitting tags in the cell, and the smaller the total interference among transmitting tags, hence the higher $\mathbb{P}_b^s$.
2) Given $\check{d}$, $\mathbb{P}_b^s$ increases as λ_w^0 decreases. The reason is similar as that in above and omitted.

In addition, we also verify the accuracy of $\mathbb{P}_b^s$ as the density λ_w^0 of underlying nodes and mean number Λ_b of tags in a subcell varies, under different settings of density λ_w^0, path-loss exponent α, average noise power σ^2, and reflection power P_0. For more details, please refer to Appendix G of Supplementary File [23].

C. Parameters Optimization

In this section, we demonstrate how to exploit our theoretical model to find the optimal parameter settings. Fig. 8 shows the backscatter throughput Γ_b versus the density of underlying nodes λ_w^0, when $\Lambda_b = 3$, $\alpha = 3$, $L = 8$, $\check{d}$ = 10 m, $\theta = 30$ dB, $P_0 = 1$ dBm, and $\sigma^2 = -100$ dBm. From this figure, we can see that Γ_b increases to a maximum value as λ_w^0 increases from 0 to 0.001 nodes/m^2 but starts decreasing when λ_w^0 continues increasing. The reason is as follows. When λ_w^0 is small, λ_w is also small, the number of concurrent tag transmissions is small, leading to a low throughput. However, when λ_w^0 is large, λ_w is also large, a great many tag transmissions will cause serious interferences, thereby lowering the throughput as well. Therefore, there exists an optimal λ_w^0 that balances concurrent tag transmissions and interferences to maximize the backscatter throughput. In this example, $\lambda_w^0 = 0.00015$ nodes/m^2 is the optimal density that maximizes Γ_b.

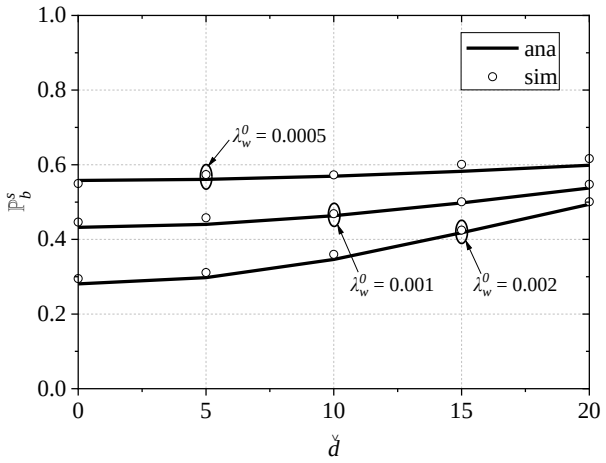

Fig. 7. $\mathbb{P}_b^s$ versus $\check{d}$ under λ_w^0 = 0.0005, 0.001, 0.002 nodes/m^2.

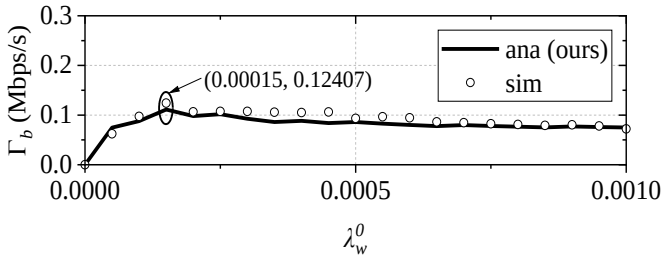

Fig. 8. Γ_b versus λ_w^0, where $\Lambda_b = 3$ tags.

VIII. Conclusion

WiFi backscatter exploits ubiquitous WiFi signals as excitation signals to convey data and hence offers wide application prospects in many fields. However, the inherent limitations of backscatter systems, such as short transmission ranges and low throughput, have motivated the development of NWB. NWB can effectively extend the communication range of backscatter tags with forwarding assistants of WiFi nodes and greatly improve the backscatter throughput by enabling concurrent transmissions of backscatter tags. This paper proposes a novel performance model LoCoR for capturing location and contention randomness, to analyze WiFi and backscatter throughputs of NWB. Our model adopts a stochastic geometry approach to characterize the WiFi nodes' repulsive attributes and backscatter tags' clustering attributes. Besides, it accounts for the randomness and dependency of WiFi and backscatter contentions. Extensive simulation results verify the accuracy of our model. This study can help engineers easily configure optimal design parameters to maximize system throughput.

Acknowledgment

The authors would like to thank the editor and anonymous reviewers for their valuable suggestions and insightful

comments. The authors would also like to thank Dr. Zhimin Wang for his help.

REFERENCES

[1] B. Kellogg, A. Parks, S. Gollakota, J. R. Smith, and D. Wetherall, "Wi-Fi backscatter: Internet connectivity for RF-powered devices," in *Proceedings of the 2014 ACM Conference on SIGCOMM*, 2014, pp. 607–618.

[2] D. Bharadia, K. R. Joshi, M. Kotaru, and S. Katti, "Backfi: High throughput wifi backscatter," *ACM SIGCOMM Computer Communication Review*, vol. 45, no. 4, pp. 283–296, 2015.

[3] X. Yang *et al.*, "A survey on smart agriculture: Development modes, technologies, and security and privacy challenges," *IEEE/CAA Journal of Automatica Sinica*, vol. 8, no. 2, pp. 273–302, 2021.

[4] G. Franze, G. Fortino, X. Cao, G. M. L. Sarne, and Z. Song, "Resilient control in large-scale networked cyber-physical systems: Guest editorial," *IEEE/CAA Journal of Automatica Sinica*, vol. 7, no. 5, pp. 1201–1203, 2020.

[5] Q. Peng *et al.*, "Reliability-aware and deadline-constrained mobile service composition over opportunistic networks," *IEEE Transactions on Automation Science and Engineering*, vol. 18, no. 3, pp. 1012–1025, 2020.

[6] Z. Ma, L. Feng, and F. Xu, "Design and analysis of a distributed and demand-based backscatter MAC protocol for internet of things networks," *IEEE Internet of Things Journal*, vol. 6, no. 1, pp. 1246–1256, 2018.

[7] P. Zhang, D. Bharadia, K. Joshi, and S. Katti, "Hitchhike: Practical backscatter using commodity wifi," in *Proceedings of the 14th ACM Conference on Embedded Network Sensor Systems CD-ROM*, 2016, pp. 259–271.

[8] T. Adame, A. Bel, B. Bellalta, J. Barcelo, and M. Oliver, "IEEE 802.11 ah: the WiFi approach for M2M communications," *IEEE Wireless Communications*, vol. 21, no. 6, pp. 144–152, 2014.

[9] E. Khorov, A. Lyakhov, A. Krotov, and A. Guschin, "A survey on IEEE 802.11 ah: An enabling networking technology for smart cities," *Computer communications*, vol. 58, pp. 53–69, 2015.

[10] Z. Wang, L. Feng, S. Yao, K. Xie, and Y. Chen, "Low-Cost and Long-Range Node-Assisted WiFi Backscatter Communication for 5G-Enabled IoT Networks," *Wireless Communications and Mobile Computing*, vol. 2021, 2021.

[11] F. Xu *et al.*, "The State of AI-Empowered Backscatter Communications: A Comprehensive Survey," *IEEE Internet Things J.*, vol. 10, no. 24, pp. 21763–21786, Dec. 2023, doi: 10.1109/JIOT.2023.3299210.

[12] T. Jiang *et al.*, "Backscatter Communication Meets Practical Battery-Free Internet of Things: A Survey and Outlook," *IEEE Communications Surveys & Tutorials*, vol. 25, no. 3, pp. 2021–2051, 2023, doi: 10.1109/COMST.2023.3278239.

[13] A. Goel and S. De, "Backscatter Communication Based Sensor Data Collection Using LASER Powered UAV," in *ICC 2023 - IEEE International Conference on Communications*, Rome, Italy: IEEE, May 2023, pp. 2896–2901. doi: 10.1109/ICC45041.2023.10278594.

[14] L. Shi, R. Q. Hu, Y. Ye, and H. Zhang, "Modeling and Performance Analysis for Ambient Backscattering Underlaying Cellular Networks," *IEEE Transactions on Vehicular Technology*, vol. 69, no. 6, pp. 6563–6577, Jun. 2020, doi: 10.1109/TVT.2020.2984529.

[15] Q. Wang, Y. Zhou, H.-N. Dai, G. Zhang, and W. Zhang, "Performance on Cluster Backscatter Communication Networks with Coupled Interferences," *IEEE Internet of Things Journal*, vol. 9, no. 20, pp. 20282–20294, Oct. 2022, doi: 10.1109/JIOT.2022.3174002.

[16] K. Han and K. Huang, "Wirelessly Powered Backscatter Communication Networks: Modeling, Coverage, and Capacity," *IEEE Transactions on Wireless Communications*, vol. 16, no. 4, pp. 2548–2561, Apr. 2017, doi: 10.1109/TWC.2017.2665629.

[17] X. Cao, Z. Song, B. Yang, M. A. Elmossallamy, L. Qian, and Z. Han, "A Distributed Ambient Backscatter MAC Protocol for Internet-of-Things Networks," *IEEE Internet of Things Journal*, vol. 7, no. 2, pp. 1488–1501, Feb. 2020, doi: 10.1109/JIOT.2019.2955909.

[18] A. Iqbal and T.-J. Lee, "Opportunistic Backscatter Communication Protocol Underlying Energy Harvesting IoT Networks," *IEEE Access*, vol. 11, pp. 89568–89580, 2023, doi: 10.1109/ACCESS.2023.3306777.

[19] X. Cao, Z. Song, B. Yang, M. ElMossallamy, L. Qian, and Z. Han, "A Distributed MAC Using Wi-Fi to Assist Sporadic Backscatter Communications," in *IEEE INFOCOM 2019-IEEE Conference on Computer Communications Workshops (INFOCOM WKSHPS)*, IEEE, 2019, pp. 780–785.

[20] Y. Wang, Q. Zhao, S. Yao, L. Feng, and H. Liang, "Performance Modeling of Tags-to-WiFi Transmissions for Contention-based WiFi Backscatter Networks," in *2022 IEEE International Conference on Networking, Sensing and Control (ICNSC)*, Dec. 2022, pp. 1–6. doi: 10.1109/ICNSC55942.2022.10004070.

[21] X. Zhang and M. Haenggi, "The Performance of Successive Interference Cancellation in Random Wireless Networks," *IEEE Transactions on Information Theory*, vol. 60, no. 10, pp. 6368–6388, Oct. 2014, doi: 10.1109/TIT.2014.2341248.

[22] S. Sen, N. Santhapuri, R. R. Choudhury, and S. Nelakuditi, "Successive Interference Cancellation: Carving Out MAC Layer Opportunities," *IEEE Transactions on Mobile Computing*, vol. 12, no. 2, pp. 346–357, Feb. 2013, doi: 10.1109/TMC.2012.17.

[23] "Analytical Modeling of Location and Contention Randomness for Node-Assisted WiFi Backscatter Communication (Supplementary Material)." [Online]. Available: https://github.com/wang-yulei/LoCoR.

[24] G. Ghatak, S. R. Khosravirad, and A. D. Domenico, "Stochastic Geometry Framework for Ultrareliable Cooperative Communications With Random Blockages," *IEEE Internet of Things Journal*, vol. 9, no. 7, pp. 5150–5161, Apr. 2022, doi: 10.1109/JIOT.2021.3108955.

[25] H. ElSawy, E. Hossain, and S. Camorlinga, "Characterizing random CSMA wireless networks: A stochastic geometry approach," in *2012 IEEE International Conference on Communications (ICC)*, Jun. 2012, pp. 5000–5004. doi: 10.1109/ICC.2012.6363772.

[26] S. D. Okegbile, B. T. Maharaj, and A. S. Alfa, "Interference Characterization in Underlay Cognitive Networks With Intra-Network and Inter-Network Dependence," *IEEE Trans. on Mobile Comput.*, vol. 20, no. 10, pp. 2977–2991, Oct. 2021, doi: 10.1109/TMC.2020.2993408.

[27] J. Park and I. Guvenc, "Interference Analysis for UAV Radar Networks With Guard Zones Based on Stochastic Geometry," *IEEE Transactions on Aerospace and Electronic Systems*, pp. 1–31, 2023, doi: 10.1109/TAES.2023.3236308.

[28] C. Lee and M. Haenggi, "Interference and Outage in Poisson Cognitive Networks," *IEEE Transactions on Wireless Communications*, vol. 11, no. 4, pp. 1392–1401, Apr. 2012, doi: 10.1109/TWC.2012.021512.110131.

[29] M. Haenggi, "Mean Interference in Hard-Core Wireless Networks," *IEEE Communications Letters*, vol. 15, no. 8, pp. 792–794, Aug. 2011, doi: 10.1109/LCOMM.2011.061611.110960.

[30] M. Haenggi, *Stochastic geometry for wireless networks*. Cambridge University Press, 2012.

[31] R. K. Ganti and M. Haenggi, "Interference and Outage in Clustered Wireless *Ad Hoc* Networks," *IEEE Trans. Inform. Theory*, vol. 55, no. 9, pp. 4067–4086, Sep. 2009, doi: 10.1109/TIT.2009.2025543.

[32] X. Peng, C. Ren, G. Chen, and L. Qiu, "Analysis of Clustered Multi-Antenna Small Cells With Intra-Cluster Interference Cancellation," *IEEE Transactions on Vehicular Technology*, vol. 68, no. 11, pp. 11343–11347, Nov. 2019, doi: 10.1109/TVT.2019.2936038.

[33] J. Tang, G. Chen, J. P. Coon, and D. E. Simmons, "Distance distributions for Matérn cluster processes with application to network performance analysis," in *2017 IEEE International Conference on Communications (ICC)*, May 2017, pp. 1–6. doi: 10.1109/ICC.2017.7997055.

[34] J. Tang, G. Chen, and J. P. Coon, "Joint Coverage Enhancement by Power Allocation in Poisson Clustered Out-of-Band D2D Networks," *IEEE Transactions on Vehicular Technology*, vol. 67, no. 12, pp. 11537–11548, Dec. 2018, doi: 10.1109/TVT.2018.2871065.

[35] V. Liu, A. Parks, V. Talla, S. Gollakota, D. Wetherall, and J. R. Smith, "Ambient Backscatter: Wireless Communication Out of Thin Air," *ACM SIGCOMM Computer Communication Review*, vol. 43, no. 4, pp. 39–50, Oct. 2013.

[36] M. Chu, A. Liu, J. Chen, V. K. N. Lau, and S. Cui, "A Stochastic Geometry Analysis for Energy-Harvesting-Based Device-to-Device Communication," *IEEE Internet Things J.*, vol. 9, no. 2, pp. 1591–1607, Jan. 2022, doi: 10.1109/JIOT.2021.3091723.

[37] X. Zhang and J. G. Andrews, "Downlink Cellular Network Analysis With Multi-Slope Path Loss Models," *IEEE Transactions on Communications*, vol. 63, no. 5, pp. 1881–1894, 2015.

[38] Y. Liu, H.-N. Dai, M. Imran, and N. Nasser, "Ground-to-UAV Communication Network: Stochastic Geometry-based Performance Analysis," in *ICC 2021 - IEEE International Conference on Communications*, Montreal, QC, Canada: IEEE, Jun. 2021, pp. 1–6. doi: 10.1109/ICC42927.2021.9500746.

[39] N. Deng, W. Zhou, and M. Haenggi, "Heterogeneous Cellular Network Models With Dependence," *IEEE J. Select. Areas Commun.*, vol. 33, no. 10, pp. 2167–2181, Oct. 2015, doi: 10.1109/JSAC.2015.2435471.

[40] G. Bianchi, "Performance analysis of the IEEE 802. 11 distributed coordination function," *IEEE Journal on selected areas in communications*, vol. 18, no. 3, pp. 535–547, 2000.
[41] A. Kumar, E. Altman, D. Miorandi, and M. Goyal, "New Insights From a Fixed-Point Analysis of Single Cell IEEE 802.11 WLANs," *IEEE/ACM Transactions on Networking*, vol. 15, no. 3, pp. 588–601, Jun. 2007, doi: 10.1109/TNET.2007.893091.
[42] Q. Zhao, D. H. Tsang, and T. Sakurai, "A simple and approximate model for nonsaturated IEEE 802.11 DCF," *IEEE Transactions on Mobile Computing*, vol. 8, no. 11, pp. 1539–1553, 2009.
[43] Q. Zhao, D. H. Tsang, and T. Sakurai, "Modeling nonsaturated IEEE 802.11 DCF networks utilizing an arbitrary buffer size," *IEEE Transactions on Mobile Computing*, vol. 10, no. 9, pp. 1248–1263, 2010.
[44] B. Błaszczyszyn, M. Haenggi, P. Keeler, and S. Mukherjee, *Stochastic Geometry Analysis of Cellular Networks*, 1st ed. Cambridge University Press, 2018. doi: 10.1017/9781316677339.

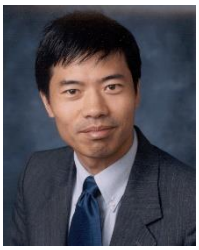

MengChu Zhou (Fellow, IEEE) received his Ph. D. degree from Rensselaer Polytechnic Institute, Troy, NY in 1990 and then joined New Jersey Institute of Technology where he is now a Distinguished Professor. His interests are in Petri nets, automation, Internet of Things, and big data. He has over 1200 publications including 17 books, 800+ journal papers (650+ in IEEE transactions), 31 patents and 32 book-chapters. He is Fellow of IFAC, AAAS, CAA and NAI.

Yulei Wang received his B.S. degree from University of Science and Technology Beijing, Beijing, China, in 2015, and M.S. degree from Macau University of Science and Technology (MUST), Macau, China, in 2019. He is pursuing the Ph.D. degree in MUST. His current research interests include wireless networks and stochastic geometry.

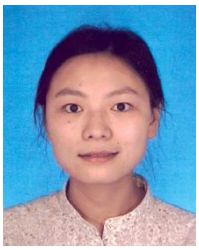

Li Feng received her M.S. degree in operation research from the Department of Mathematics, University of Hong Kong, Hong Kong, in 2007, and her Ph.D. degree in electronic information technology from the School of Computer Science and Engineering (SCSE), Macau University of Science and Technology (MUST), Macao, China, in 2013. She is currently an Associate Professor in SCSE, MUST. Her current research interests include Internet of Things, wireless and mobile networks, power saving, software defined networking, and performance analysis.

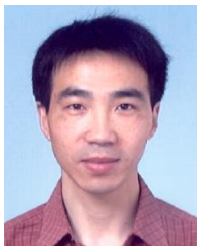

Qinglin Zhao received his Ph.D. degree from the Institute of Computing Technology, the Chinese Academy of Sciences, Beijing, China, in 2005. From May 2005 to August 2009, he worked as a postdoctoral researcher at the Chinese University of Hong Kong and the Hong Kong University of Science and Technology. Since September 2009, he has been with the School of Computer Science and Engineering at Macau University of Science and Technology and now he is a professor. He serves as an associate editor of IEEE Transactions on Mobile Computing and IET Communications. His research interests include blockchain and decentralization computing, machine learning and its applications, Internet of Things, wireless communications and networking, cloud/fog computing, software-defined wireless networking.

Peiyun Zhang (M'16–SM'17) received her Ph.D. in computer science from the School of Computer Science and Technology at the Nanjing University of Science and Technology, Nanjing, China in 2008. She is currently a professor at the Engineering Research Center of Digital Forensics of Ministry of Education, and the School of Computer Science, Nanjing University of Information Science & Technology. Her interests include blockchains, and cloud/ trust computing. She has published over 70 papers in these fields.

Shumin Yao received his Ph.D. and M.S. degrees from Macau University of Science and Technology, Macau, China, in 2022 and 2018, respectively, and his B.S. degree from Beijing Institute of Technology, Zhuhai, China, in 2016. He is currently a Postdoctoral researcher in Peng Cheng Laboratory, Shenzhen, China. His interests include wireless LAN and Internet of Things.